Oscillatory Entrainment of Thalamic Neurons by Theta Rhythm in Freely Moving Rats

Marian Tsanov, Ehsan Chah, Nick Wright, Seralynne D. Vann, Richard Reilly, Jonathan T. Erichsen, John P. Aggleton and Shane M. O'Mara

J Neurophysiol 105:4-17, 2011. First published 20 October 2010; doi:10.1152/jn.00771.2010

J Neurophysiol 105: 4–17, 2011.
First published October 20, 2010; doi:10.1152/jn.00771.2010.

Oscillatory Entrainment of Thalamic Neurons by Theta Rhythm in Freely Moving Rats

Marian Tsanov,[1,2] Ehsan Chah,[1,3] Nick Wright,[4] Seralynne D. Vann,[4] Richard Reilly,[1,3] Jonathan T. Erichsen,[5] John P. Aggleton,[4] and Shane M. O'Mara[1,2]

[1]*Trinity College Institute of Neuroscience,* [2]*School of Psychology, and* [3]*Trinity Centre for Bioengineering, Trinity College, Dublin, Ireland; and* [4]*Schools of Psychology and* [5]*Optometry and Vision Sciences, Cardiff University, United Kingdom*

Submitted 8 September 2010; accepted in final form 20 October 2010

Tsanov M, Chah E, Wright N, Vann SD, Reilly R, Erichsen JT, Aggleton JP, O'Mara SM. Oscillatory entrainment of thalamic neurons by theta rhythm in freely moving rats. *J Neurophysiol* 105: 4–17, 2011. First published October 20, 2010; doi:10.1152/jn.00771.2010. The anterior thalamic nuclei are assumed to support episodic memory with anterior thalamic dysfunction a core feature of diencephalic amnesia. To date, the electrophysiological characterization of this region in behaving rodents has been restricted to the anterodorsal nucleus. Here we compared single-unit spikes with population activity in the anteroventral nucleus (AV) of freely moving rats during foraging and during naturally occurring sleep. We identified AV units that synchronize their bursting activity in the 6–11 Hz range. We show for the first time in freely moving rats that a subgroup of AV neurons is strongly entrained by theta oscillations. This feature together with their firing properties and spike shape suggests they be classified as "theta" units. To prove the selectivity of AV theta cells for theta rhythm, we compared the relation of spiking rhythmicity to local field potentials during theta and non-theta periods. The most distinguishable non-theta oscillations in rodent anterior thalamus are sleep spindles. We therefore compared the firing properties of AV units during theta and spindle periods. We found that theta and spindle oscillations differ in their spatial distribution within AV, suggesting separate cellular sources for these oscillations. While theta-bursting neurons were related to the distribution of local field theta power, spindle amplitude was independent of the theta units' position. Slow- and fast-spiking bursting units that are selectively entrained to theta rhythm comprise 23.7% of AV neurons. Our results provide a framework for electrophysiological classification of AV neurons as part of theta limbic circuitry.

INTRODUCTION

The anterior thalamic nuclei appear to be vital for human episodic memory (Aggleton and Sahgal 1993; Gold and Squire 2006; Harding et al. 2000); animal lesion experiments (including cross-disconnection studies) confirm the critical role of these nuclei for hippocampal-dependent learning (Parker and Gaffan 1997; Warburton et al. 2001). Of the rodent anterior thalamic nuclei, only the electrophysiological properties of the anterodorsal (AD) nucleus are well described, a consequence of its role within the head-direction circuit (Taube 2007). In contrast, electrophysiological information concerning the other nuclei (anteromedial, anteroventral) remains scarce even though this information may explain the significance of these thalamic relays for hippocampal-dependent memory. Here we seek to address the lacuna in the literature by recording the electrophysiological responses of rat anteroventral (AV) neurons, using chronically implanted microelectrodes. We attempt the first classification of AV unit activity in the freely moving animal by classifying the recorded units according to their firing rate, interspike intervals, and spiking rhythmicity.

Intracellular recordings show that AV neurons have intrinsic membrane properties similar to those of other thalamocortical neurons (Jahnsen and Llinas 1984b; Pare et al. 1987), yet AV neurons may differ from the rest of thalamus because of their predisposition to rhythmic discharges (Bland et al. 1995). Single-unit recordings from AV and the anteromedial (AM) thalamic nuclei in urethan-anesthetized rats indicate that some AV neurons tend to fire in theta-rhythmic manner (Vertes et al. 2001). This discovery is significant as theta rhythm in the limbic system may serve to modulate episodic memory formation (Buzsáki 2002, 2005; Hasselmo and Eichenbaum 2005). Additionally, the anterior thalamic nuclei are hypothesized to be an interface between limbic theta activity during active behavior and thalamic oscillatory mode, characterized by sleep spindles. The reticular nucleus, a generator of spindling rhythmicity (Steriade et al. 1985, 1987), projects to rodent anterior thalamic nuclei (Gonzalo-Ruiz and Lieberman 1995), leaving open the question of the relationship between generators of spindle oscillatory activity and theta rhythm within AV. We hypothesized that the distribution of theta and spindle local spectral power within AV are independent as they are triggered by different sources. Here we recorded single units from AV in freely moving rats (previous studies have used urethan anesthesia) during active and sleep-associated behavioral states. To demonstrate that theta rhythm is a locally induced oscillation, unlike spindle oscillations, we compared the spectral power distribution of both rhythms across all tetrodes implanted in AV, and we also evaluated theta units' contribution to both oscillations. We used small-diameter, high-impedance electrodes to target the field activity from a small number of cells in a nonlayered structure (Berke et al. 2004), allowing localization of the signal in close proximity to the electrode tip (Buzsaki 2004; Pesaran 2009). For larger-scale estimates of AV low-frequency oscillations, we used a large-diameter, low-impedance electrode. We investigated the contribution of the rhythmical cellular bursts to the local and global oscillatory

Address for reprint requests and other correspondence: S. M. O'Mara: Trinity College Institute of Neuroscience, Trinity College Dublin, Dublin 2, Ireland (E-mail: smomara@tcd.ie).

spectral power of anterior thalamus. We show that AV units are related to the amplitude of the theta but not to the spindling rhythm. Our large-scale recordings confirm the theta oscillatory patterns of AV and suggest the anterior thalamus as a component of the limbic theta circuit.

METHODS

Surgical implantation of electrodes

The recording electrodes consisted of four bundles of four platinum-iridium wires (90% platinum, 10% iridium; HM-L insulated, 25 μm bare wire diameter, California Fine Wire) twisted together. Tetrodes were threaded through a 25 gauge guide cannula and protected with a 21 gauge cover. Tetrodes were then mounted in a small microdrive (Axona) and implanted in the anteroventral thalamus (-1.6 AP, -1.4 ML and 4.5 mm ventral to dura).

The microdrive was fixed with dental acrylic (Associated Dental, Swindon, UK) applied to the anchor screws inserted in the skull. The anchor screw located on the left frontal bone was used as a grounding point. The single-unit recordings were referenced to tetrode wire implanted together with the recording tetrodes (Anderson and O'Mara 2003; Gray et al. 1995). For the simultaneous LFP recordings of small- and large-diameter electrodes, we added large-diameter electrode (100 μm) in the guide cannula. The intracranial length of all electrodes was the same, and they were simultaneously lowered into anterior thalamus by the microdrive in 50 μm steps. Experiments were conducted in accordance with European Community directive, 86/609/EC, and the Cruelty to Animals Act, 1876, and followed Bioresources Ethics Committee, Trinity College, Dublin, Ireland, and international guidelines of good practice.

Recording techniques

We used only 4 tetrodes (16 channels in total) to protect thalamic tissue from the destructive side effect of electrode implantation. Large numbers of neurons are likely to be damaged by the blunt end of the closely spaced electrode wires (Buzsaki 2004). Thus only a small fraction of the neurons can be reliably separated with currently available probes and spike sorting algorithms (Csicsvari et al. 1999; Harris et al. 2003; Wilson and McNaughton 1993). This choice of implantation was related to our purpose of evaluating the contribution of extracellularly recorded activity to the LFP signal. After $\geq$1 wk recovery, subjects were connected, via a 16 channel headstage (Axona) to a recording system that also allowed for animal position tracking. Signals were amplified (10,000–30,000 times) and band-pass filtered between 380 Hz and 6 kHz for single-unit detection. To maximize cell separation, only waveforms of sufficient amplitude ($\geq$3 times noise threshold) were acquired. Candidate waveforms were discriminated off-line using graphical cluster-cutting software (Axona), which allows waveform separation based on multiple features including spike amplitude, spike duration, maximum and minimum spike voltage, and the time of occurrence of maximum and minimum spike voltages. Autocorrelation histograms were built for each unit, and the whole unit was removed from the analysis if the histogram revealed the existence of correlations within the first 2 ms (refractory period), inconsistent with good unit isolation. Autocorrelograms were plotted between $-50/-700$ and 50/700 ms with a bin width of 1 ms. To measure the degree of spiking rhythmicity, we calculated the ratio of the maximal amplitude of sinusoidal fitted curve to the maximal value of the nonsinusoidal fitted curve of the autocorrelograms. A sine wave with decaying amplitude was fitted to the autocorrelograms shown in *Eq. 1* (excluding the peak around 0)

$$\left[a\left(\sin\left(\omega t\right)+1\right)+b\right]\cdot e^{\frac{-|t|}{\tau_1}} \quad (1)$$

The Theta index is defined as the ratio of the fitted parameters, *a/b* (Royer et al. 2010), where *a* is amplitude of oscillation and *b* is the offset of the oscillation.

Recording sessions

The recordings took place in a square arena (64 $\times$ 64 $\times$ 25 cm high) situated in the center of a room with multiple background cues available (surrounding curtains were open). Rats were placed in the open field and 20 mg food pellets (TestDiet, Formula 5TUL) were thrown in every 20 s to random locations within the open field; in this way, animals were in continuous locomotion, allowing for complete sampling of the environment. For spindle recordings, pellet-throwing was discontinued, and the rats were allowed to rest. Each experimental session was 16 min. The definition of theta and spindle periods was based on off-line detection of characteristic LFP waveforms.

We identified 147 well-isolated units within the anterior thalamic nuclei from nine male (250–350 g) Lister-Hooded rats (Harlan). Based on electrophysiological and postmortem histological criteria, we estimated that 80 of these units were from anteroventral nucleus (AV), whereas 67 were from anterodorsal nuleus (AD) or from laterodorsal thalamic nucleus, ventrolateral part (LDVL; Fig. 1*A*).

Postmortem verification of electrode site

At the end of the study, brains were removed for histological verification of electrode localization. The animals underwent transcardial perfusion with 0.1 M PBS followed by 10% formol-saline. The brains were postfixed in 10% formol-saline and then transferred to 25% sucrose overnight. Brain sections (16 μm) were stained according to the Nissl method using 1% toluidine blue, and then examined using a light microscope. Data from brains in which incorrect electrode localization was found (e.g., anterodorsal thalamic nucleus or ventral anterior thalamic nucleus) were excluded.

Statistical analyses

All data were analyzed using Prism software (GraphPad Software, La Jolla, CA). Statistical significance was estimated by using two-tailed *t*-test, two-way ANOVA paired with Tukey posttest. The probability level interpreted as statistically significant was $P < 0.05$. For the correlation analyses, we used Pearson's coefficient. For the experiments where we correlated the large-diameter-recorded local field potential (LFP_l) and small-diameter-recorded local field potential (LFP_s) signal, we used epochs with bin size of 1 s. LFP signals were sampled at 0.5 kHz and stored for further off-line analysis. Fourier analysis of artifact-free 1-s-long epochs was performed with the Hanning window function using Matlab. The absolute values of spectral power for each pair of LFP_l and LFP_s signals were normalized and then correlated for the entire recording of 16 min (960 bins per recording in total).

Recording volume of the LFP_l and LFP_s

Our goal was to evaluate the approximate contribution of AV synchronized activity to recorded thalamic LFP_l (larger-diameter electrode: 100 μm, with impedance: 50–250 kΩ) and LFP_s signals (small diameter electrode: 25 μm, with impedance: 1–1.5 MΩ) under our experimental conditions. The amplitude of intracellularly measured thalamic membrane potential oscillations during synchronized states can reach values of 1/4 to 1/3 (0.285 on average) of the amplitude of the spike (Contreras et al. 1997b; Fuentealba et al. 2004; Steriade et al. 1993). The conductive properties of excitable membranes preserve the same ratio when

measured extracellularly (Ylinen et al. 1995), for which we take the value of 0.285 for peak oscillation amplitude to peak spike as a point source. A point source is a single identifiable localized source of certain signal and neurons are accepted point sources for the extracellularly recorded currents (Csicsvari et al. 2003). We then model the thalamic neuron as a point source with peak

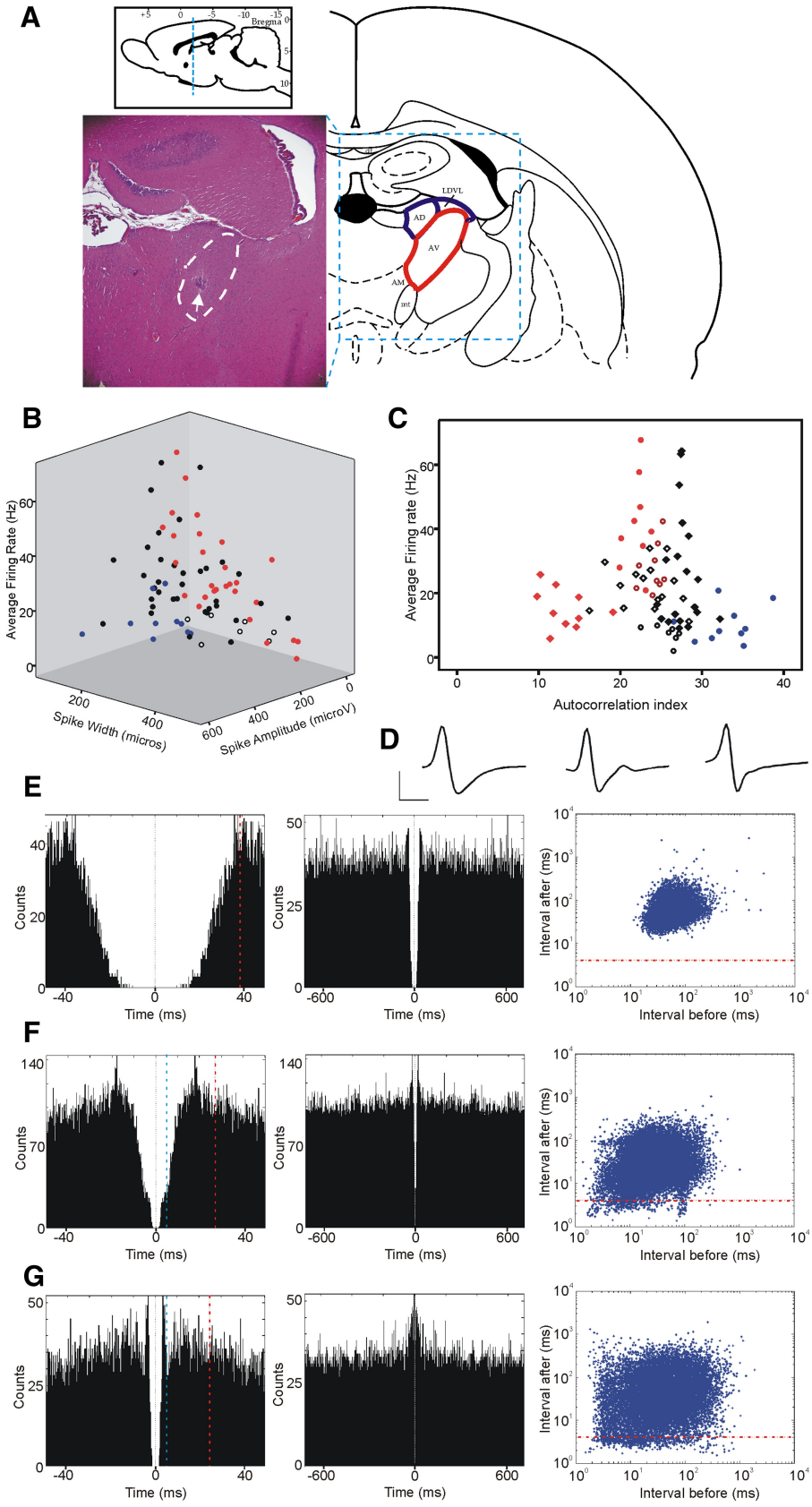

FIG. 1. Properties and distribution of major anteroventral nucleus (AV) neuron classes. *A*: Nissl-stained coronal brain section from a rat where four chronically implanted tetrodes targeted the AV (highlighted with white dashed line). White arrow, the tip of the tetrodes surrounded by a small area of gliosis. The histological section lies within coronal plane with anterio-posterior coordinates of -1.7 ± 0.2 mm from Bregma (*top inset*). Rat AV (marked with red on the atlas schematic, right) is located ventrally to the anterodorsal nucleus (AD) and laterodorsal thalamic nucleus, ventrolateral part (LDVL; both nuclei marked with blue). *B*: 3-dimensional (3D) scatter plot of electrophysiological parameters for 80 AV neurons (9 rats), recorded during behaviorally active periods. We used 3 parameters to represent AV characteristics: average firing frequency (Hz), spike width (μs), and spike amplitude (μA). Nonbursting units are blue, theta-rhythmical units red, nonclassified units are white, and nontheta bursting units are black. Although spike amplitude depends on the proximity of the tetrode to the recorded unit, we have included this parameter because of its characteristically low values for theta-rhythmic units (143 ± 43.8 μA). *C*: AV neuronal diversity: we plot here the average firing rate (y axis) against the mean value (1st moment) of the spike autocorrelogram (Csicsvari et al. 1998), the autocorrelation index (x axis). All unit classes formed distinct clusters: slow-spiking theta bursters (red rectangles, $n = 10$); fast spiking theta bursters (red dots, $n = 9$); theta-modulated bursters (brown circles, $n = 9$); low-probability bursters (black rectangles, $n = 19$); nonbursters (blue dots, $n = 10$). The exceptions were high-probability nontheta bursters (white rectangles, $n = 16$), which had a less-defined distribution. Finally, nonclassified neurons are presented as white circles ($n = 7$). *D*: representative waveforms for the main AV classes described below: nonbursting (*left*), low-probability bursing (*middle*), and high-probability bursing (*right*) neurons. Horizontal scale bar: 300 μs, vertical bar 300 μV. *E*: firing properties of nonbursting AV unit from 16 min recording during active behavioral state. *Left image*: an example of 50 ms autocorrelogram; dashed vertical red line, the value of autocorrelation index. *Middle image*: 700 ms autocorrelogram of the same unit. *Right image*: 2D log-scale interspike interval (ISI) scatterplot for the same neuron. The points below the dashed horizontal red line represent the action potentials within bursts. *F*: representative example of 50 ms (*left*) and 700 ms (*middle*) autocorrelogram and ISI scatterplot (*right*) for low-probability bursting AV unit. *G*: representative example of 50 ms (*left*) and 700 ms (*middle*) autocorrelogram and ISI scatterplot (*right*) for high-probability bursting AV unit. The distance between *time 0* and 1st 5 ms (marked with blue vertical dashed line) in the 50 ms autocorrelogram denotes the proportional number of spike counts within the bursting range.

oscillation amplitude. The first step in the approximation of the neuronal number mediating the signal of our recordings is the estimation for a homogeneous medium that the amplitude of the source signal is decaying according to

$$V(r) = \frac{V}{r^2} \quad (2)$$

The peak amplitude of 150 μV (estimated as 0.285 times from the peak amplitude of the recorded spikes) decreases with distance from the electrode as show in *Eq. 2*. The minimum detectable change of our recording systems (Axona, A-M system) is ~5 μV; therefore we used a "point electrode" where the maximum distance between the source and point electrode for an amplitude higher than 5 μV is $r_{\text{pointelectrode}}$ ~110 μm.

We assume the electrode can be modeled by infinite point electrodes and that the calculated $r_{\text{pointelectrode}}$ corresponds to the point on the electrode closest to the source, i.e., the edges of the electrode determine the listening volume of the electrode as a cylinder $V = \pi r^2 h$, where r and h represent the radius and height of the cylinder.

The approximate estimation of h for AV in 300 g rat is ~1 mm, which we accept as a homogenous structure and is constant for both type of electrodes. Then the only variable varying is the radius r, which is the sum of $r_{\text{pointelectrode}}$ and the radius of the electrode

$$\mathrm{r} = \mathrm{r}_{\text{pointelectrode}} + \mathrm{r}_{\text{electrode}} \quad (3)$$

In this study, the radius $r_{\text{electrode}}$ for small-diameter electrode was 12.5 μm and for large-diameter the radius was 50 μm. Thus we obtain values for r (using *Eq. 3*) of 122.5 and 160, respectively. Then the recorded area is a cylinder with volume V_s = 0.0471 mm^3 for the small-diameter and V_l = 0.0804 mm^3 for the large-diameter electrode. The average density of rodent dorsal thalamus is ~23,000 neurons per mm^3 (Mooney and Miller 2007; Ramos et al. 1995), which translates to ~1,083 local neurons that contribute to LFP_s and ~1,849 neurons to LFP_l, respectively. Our model is coherent with the passive neuronal electrical parameters known to undergo fast amplitude decay, which is proportional to the square of the distance to the point source (Pettersen and Einevoll 2008). We have to point out the approximate nature of this calculation, which is based on what will be the local input to the recorded signal, but we did not include the long-scale currents from neighboring structures or even the entire brain.

Next we estimated the role of electrode impedance on the recorded signal. We analyzed the resistance values of the recording setup to evaluate the effect of the electrode impedance on the voltage sensed by the amplifier (Nelson et al. 2008). Because the resistance of the amplifier (>10 MΩ) used in our study (Axona and A-M System) is much larger than the electrode resistance, we can conclude that the effect of electrode impedance on the signal amplitude is negligible. Resistance of the electrode is, however, directly proportional to the amount of thermal noise produced by the electrode. Using the resistor's absolute temperature, the resistance of the electrode and the bandwidth of the frequencies of interest (Huigen et al. 2002), we estimated that the thermal noise by the electrode is 0.5–1 μV for the LFP_l electrode and 2- 2.3 μV for the LFP_s electrode. As both values are beyond the minimum detectable change of our recording systems (Axona, A-M System), we can conclude that the resistance of the electrodes has a negligible effect on the recorded signal.

RESULTS

Distinct classes of AV neurons in freely moving rats

We combined electrophysiological and anatomical approaches to identify AV units. AV lies beneath the anterodorsal nucleus (Fig. 1*A*), which contains predominantly head-direction cells (Taube 1995). From 147 well-isolated units in the anterior thalamic nuclei, we confirmed 80 units from nine rats with postmortem histological verification to be within AV. Thalamic neurons are homogenous in terms of morphology (Jones 1985) and electrophysiological properties (Jahnsen and Llinas 1984a; Steriade et al. 1997), thus restricting the extracellular differentiation of neuronal clusters based only on the spike's shape and frequency (Fig. 1*B*). To distinguish cell classes within AV, we also measured the spiking autocorrelation (Fig. 1, *C* and *E*) and ISI (*E*). The great majority of AV cells were classified as bursting (70/87.5%), based on their ability to discharge with an ISI of <5 ms, while relatively few (10/12.5%) were classified as nonbursters (Fig. 1*E,* Table 1). The bursting units revealed different profiles of activity, forming two subgroups of low- versus high-propensity-to-burst units (Fig. 1, *F* and *G, left*). The ISI plots (Fig. 1, *F* and *G, right*) show that the vast majority of the action potentials possess tonic firing properties. The action potentials located under the red horizontal line occur within the 4 ms range that defines bursting mode. Among the high-probability bursting cells, we identified neurons that fire in a rhythmic manner with a frequency of 6–11 Hz (theta range; Fig. 2). Depending on their average firing rate and their autocorrelogram profile, we subclassified the theta-bursting cells as fast (40.9 ± 15.3 Hz, Fig. 2*A*, Table 1)- or slow-spiking (14.9 ± 6.9 Hz, *B,* Table 1). Additionally, a third subgroup of bursting cells that fired only partially in a theta-rhythmic manner (Fig. 2*C*) completed the diversity of neuronal types recorded in AV (theta-modulated cells).

To quantify theta unit rhythmicity of AV cells, we fitted a sinusoidal function to the autocorrelogram of detected spikes of each neuron and used the relative amplitude of the sinusoid component as an index of theta rhythmicity (Royer et al. 2010). Theta index represents the maximal amplitude of sinusoidal fitted curve to the maximal value of the nonsinusoidal fitted curve of the autocorrelograms (see *Eq. 1,* METHODS). Thus this parameter provides information on how rhythmic is the spiking activity of the neurons in the theta frequency range. This theta index was highest for slow-spiking theta-bursting cells (0.49 ± 0.33), suggesting that this group fired mostly during theta

TABLE 1. *Electrophysiological classification of anteroventral thalamic units in freely behaving rats*

Cell types	Nonbursting	Bursting-Low Probability	Bursting-High Probability Nontheta	Theta-Bursting (Fast Spiking)	Theta-Bursting (Slow Spiking)	Bursting-Theta Modulated	Nonclassified
n	10	19	16	9	10	9	7
Average frequency, Hz	9.8 ± 5.9	29.6 ± 19.1	22.7 ± 7.3	40.9 ± 15.3	14.9 ± 6.9	27.4 ± 7.6	7.6 ± 3.3
Mean spike width, μs	174.9 ± 51.8	196.8 ± 76.3	237.4 ± 115.3	175.1 ± 49.9	382.6 ± 102.5	293.3 ± 67.2	313.3 ± 66.3
Auto-correlation index	32.7 ± 3.7	27.5 ± 1.8	23.4 ± 3.4	22.1 ± 1.4	13.2 ± 3.0	24.2 ± 1.4	26.5 ± 0.5
Theta index	—	—	—	0.11 ± 0.06	0.49 ± 0.33	0.03 ± 0.02	—

Values are ± SE.

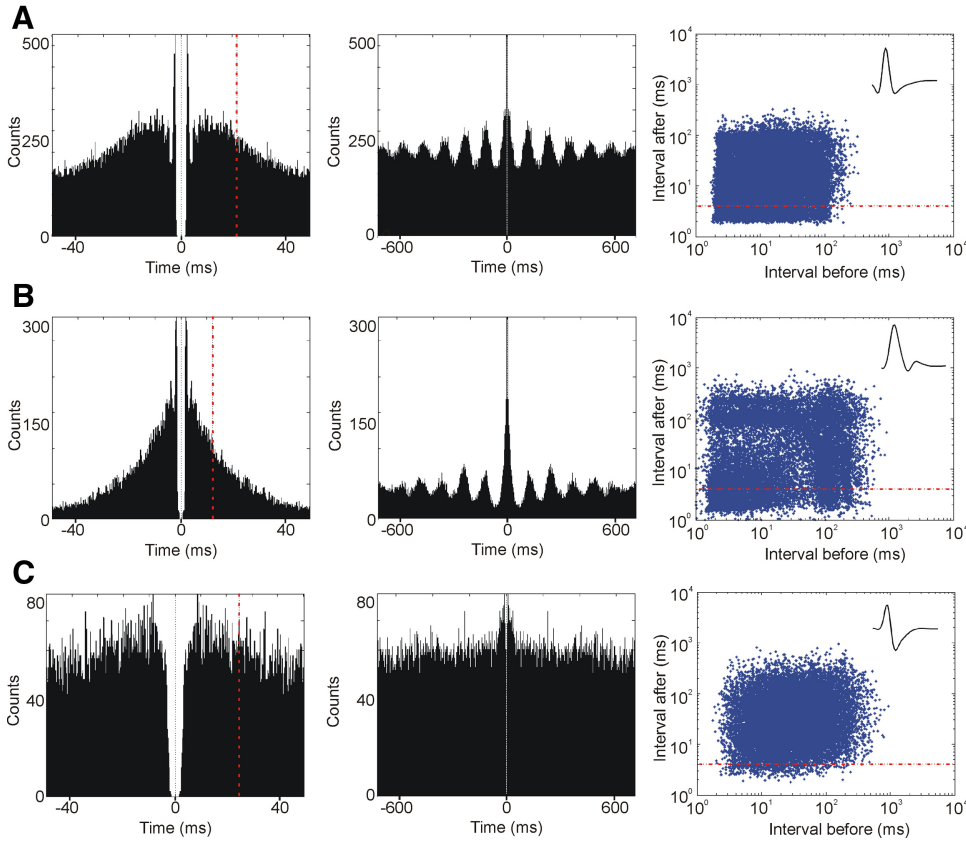

FIG. 2. Bursting properties of theta-rhythmic neurons in anteroventral thalamic nucleus. *A*: firing properties of theta-bursting fast-spiking AV unit from 16 min recording during the active behavioral state. *Left*: an example of 50 ms autocorrelogram; the dashed vertical red line indicates the value of autocorrelation index − the mean 1st moment of the histograms (Csicsvari et al. 1998). *Middle*: the 700 ms autocorrelogram of the same unit, allowing us to detect the theta rhythmicity of the recorded unit. The calculation of theta index is based on the relative amplitude of the sinusoid component of the autocorrelogram (Royer et al. 2010). *Right*: a 2D log-scale interspike interval (ISI) scatterplot for the same neuron. The abscissa indicates the interval to the previous action potential and the ordinate indicates the interval to the next one. The points below the dashed horizontal red line represent the action potentials within bursts. *B*: firing properties of a theta-bursting slow-spiking AV unit from 16 min recording during the active behavioral state. Representative examples of 50 ms (*left*) and 700 ms (*middle*) autocorrelograms and interspike interval scatterplot (*right*). *C*: firing properties of a theta-modulated AV unit from 16 min recording during the active behavioral state, shown with a representative example of 50 ms (*left*) and 700 ms autocorrelograms (*middle*). Theta rhythmicity is not visually detectable and here is based on the theta index values. *Right*: is the interspike interval scatterplot for the same unit. *Top insets, right*: representative waveforms for theta-bursting fast-spiking (*top*), theta-bursting slow-spiking (*middle*), and theta-modulated (*bottom*) neurons recorded extracellularly from rat AV.

episodes (see METHODS, Table 1). The theta index for fast-spiking theta-bursting cells (0.11 ± 0.06) shows they are continuously spiking with synchronization of their bursts within 6–11 Hz during theta episodes. Occasional firing in the theta range of otherwise theta-unrelated spiking is a feature of the theta-modulated cells with a lower theta index (0.03 ± 0.02). Overall, neurons firing predominantly in a rhythmical mode of 6–11 Hz (slow- and fast-spiking cells) comprise about a quarter (19/23.7%) of recorded AV units.

The fact that AV is characterized by a theta unit population is evident when it is compared with other anterior thalamic nuclei. For purposes of comparison, we also recorded 67 units from AD and LDVL. From these recordings only five units (7.5%) were classified as theta-bursting cells, all of which being slow-spiking (15.8 ± 9.2 Hz) with theta index 35.2 ± 8.1. The predominant population of AD and LDVL cells (55/82.1%) expressed behaviorally head-directional properties (Supplemental Fig. S1[1]). The head-direction cells were slow spiking (26/38.8%, 20.4 ± 6.4 Hz, Supplemental Fig. S1*B*) and fast spiking (29/43.3%, 39.2 ± 5.1 Hz, Supplemental Fig. S1*C*), while the rest of the AD/LDVL identified units (7/10.4%, 11.5 ± 4.9 Hz) were nonbursters.

Rhythmicity of theta unit bursting decreases during spindle periods

Thalamic neurons fire in two distinct modes: tonic and bursting (Deschenes et al. 1984; Fanselow et al. 2001; Jahnsen and Llinas 1984a). Thalamic bursts occur predominantly during slow-wave sleep, an oscillatory synchronized brain state (Weyand et al. 2001), whereas some theta unit types in limbic structures tend to fire in bursts more often during waking, active behavioral states (Klausberger et al. 2003). We compared the bursting properties of AV theta units during synchronized and desynchronized states. For the desynchronized (waking) state, we included all theta periods (Fig. 3, *A* and *B, left*). For the synchronized (sleeping) state, we included all spindle periods (*A* and *B, right*), which we identified off-line from the local field signal. Unlike spindle periods, the slow-wave sleep and the REM periods had no detectable oscillatory amplitude in thalamic extracellular local field potentials.

[1] The online version of this article contains supplemental data.

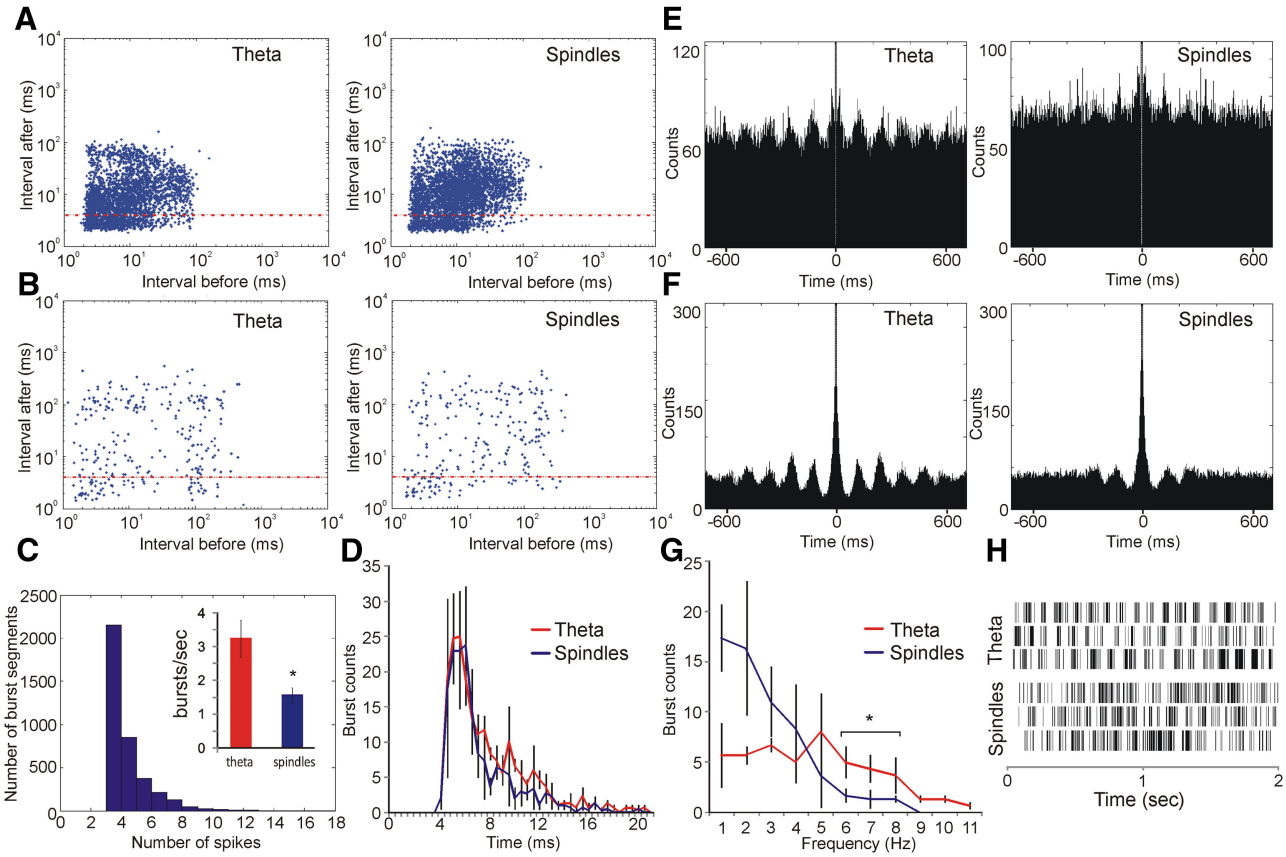

FIG. 3. Thalamic theta units express a smaller degree of bursting during spindle periods. *A*: log-scale ISI histograms for a representative fast-spiking theta unit during theta (*left*) and spindle (*right*) periods. *B*: log-scale ISI histograms for representative slow-spiking theta unit during theta (*left*) and spindle (*right*) periods. The red horizontal line denotes the units within bursting mode. *C*: estimation of burst length for fast-spiking theta cells. The majority of burst segments are composed of 3 spikes. *Right inset*: the higher number of bursts (defined as 3 consecutive spikes with an interspike duration of 4 ms) per second during theta periods (red) compared with spindle periods (blue; $P < 0.05$). *D*: theta (red) and spindle (blue) periods share similar bursts duration ($P > 0.05$). The highest number of burst counts occurs for the length of 4–7 ms for both periods. *E*: representative 700 ms autocorrelogram of a fast-spiking theta unit during theta periods (*left*) compared with spindle periods (*right*). *F*: representative 700 ms autocorrelogram of a slow-spiking theta unit during theta periods (*left*) compared with spindle periods (*right*). *G*: burst frequency histogram reveals a predominantly low frequency of the burst counts for spindle periods (blue), compared with theta periods (red). *H*: state-dependent firing pattern of thalamic theta units. Two second duration plots of spike times for 3 fast-spiking units recorded from AV during theta periods (*top*) and spindle periods (*bottom*).

Fast-spiking theta units showed a higher degree of bursting during theta periods (3.23 ± 0.95 burst/s) compared with subsequent spindle periods (1.43 ± 0.41 burst/s; Fig. 3*C*, Student's *t*-test $P < 0.05$). The increased degree of bursting was not due to prolonged duration of the bursts as the burst-length histogram showed no significant change in burst length between the two states (Fig. 3*D*, ANOVA, $F < 1$, $P > 0.05$). Burst length was defined as the time from the first to last spike within each burst. The major difference was expressed in the rhythmicity of bursts (Fig. 3, *E* and *F*), where theta periods are characterized by more frequently occurring bursts than spindle periods (Fig. 3, *G* and *H*). Autocorrelogram rhythmicity, measured by the theta index, was lower for fast-spiking theta units (Fig. 3*E*, Student's *t*-test $P < 0.01$) and slow-spiking theta units (*F*, Student's *t*-test $P < 0.01$) during spindle periods. The burst frequency histogram shows there are predominantly 1–3 burst/s during spindle periods, with no more than 8 burst/s (Fig. 3*G*). Theta periods show a similar degree of bursting at all frequencies, with a significant increase in the range of 6–11 Hz range, compared with spindle periods (Fig. 3*G*, Tukey $P < 0.05$). The increased bursting activity in the theta range reflects preburst pauses of the same rate during theta periods (Fig. 3*H*).

Graded intensity of theta oscillations matches the distribution of fast-spiking theta units

The functional impact of theta units can be represented by their influence on the theta amplitude of the LFP. Depending on the electrode properties and their localization, the neuronal area that generates the LFP ranges from a few hundred micrometers to a few millimeters (Katzner et al. 2009; Kreiman et al. 2006). We used small-diameter, high-impedance electrodes to target the LFP from a small number of cells in what is a nonlayered structure (Berke et al. 2004) and large-diameter, low-impedance electrodes to provide a large-scale estimate of the LFP (Logothetis et al. 2007). Therefore our initial aim was to restrict the volume of recorded tissue so that the field signal reflects the activity of a restricted and localized neuronal population. For this purpose, we used electrodes of small diameter (25 μm) and high impedance (1–1.5 MΩ) arranged in a tetrode configuration. Considering the small percentage of theta units in AV, we reasoned that oscillatory patterns measured with small-diameter electrodes might vary, depending on the proximity of each tetrode to the nearby theta unit. The LFP_s analyses of all rats showed that the amplitude of theta

spectral power is higher when recorded from a tetrode, used to isolate a theta unit, compared with tetrodes that are not able to detect theta units (Fig. 4, *A* and *B, left,* and *C* and *D,* Student's *t*-test $P < 0.05$). In the cases where theta units were recorded from more than one tetrode, theta spectral power still reflected the proximity of the units although the heterogenity of the signal along all tetrodes was less apparent (Fig. 5). The bursting activity of theta units was phase-locked to the trough of the local field oscillation, which was evident during robust theta epochs (Fig. 4*B*). Our data

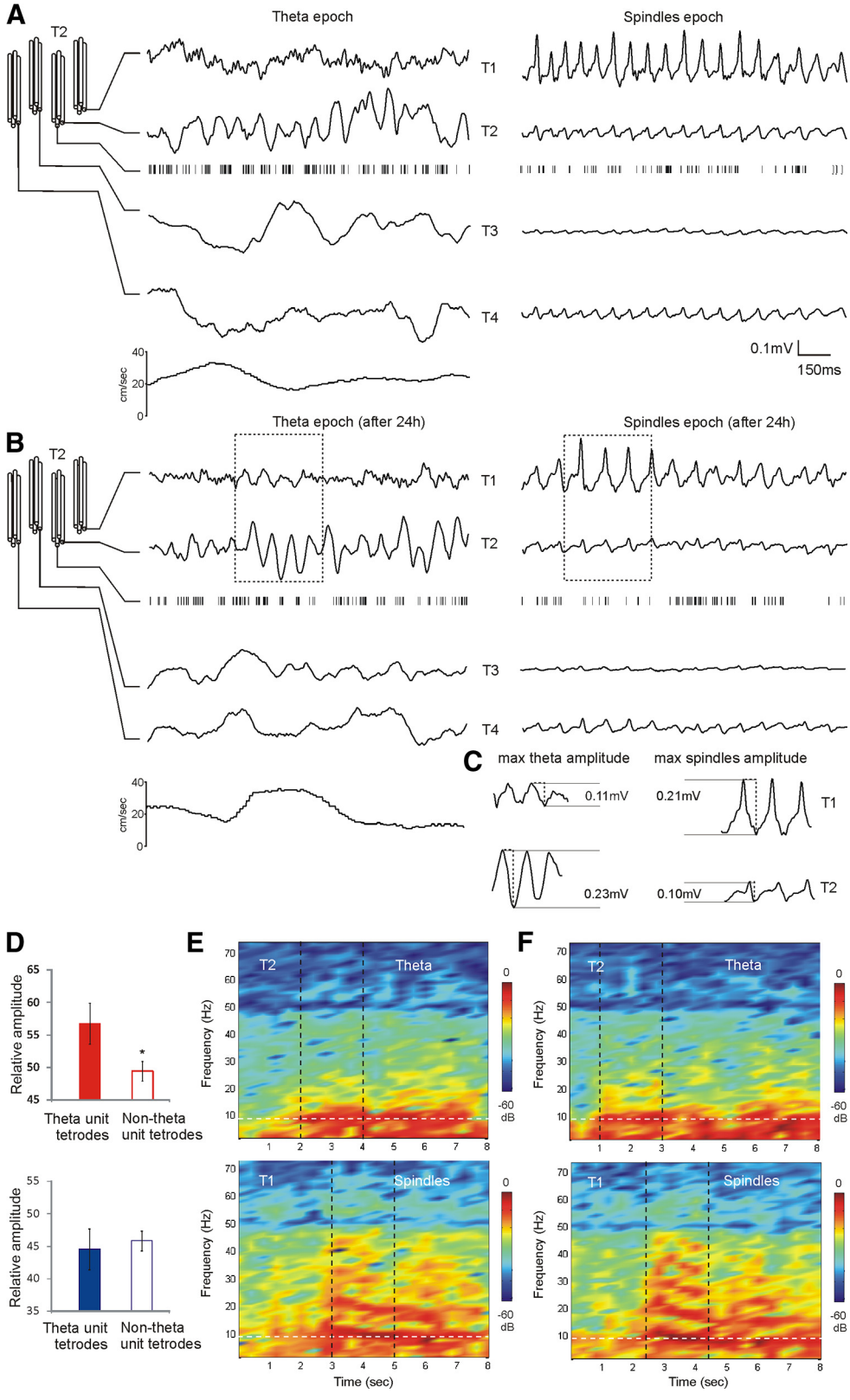

FIG. 4. Proximity of theta units determines the amplitude of theta rhythm in AV. *A*: configuration of the implanted tetrodes within AV and example of concurrent small-diameter-recorded local field potential (LFP_s) signals during theta (*left*). The most prominent theta amplitude is evident on the 2nd tetrode (T2), where a fast-spiking theta unit is also isolated. *Bottom trace*: the speed of the animal (cm/s). *Right*: the LFP_s signal from the same tetrodes during an inactive behavioral period of the animal. The presence of high-voltage spindles LFP_s defines this epoch as a spindle period. *B*: the same example 24 h later demonstrates the stability of the signal for both theta and spindle periods. Note that while tetrode 2 has the largest theta amplitude, in the following spindle period the amplitude of the sleep-associated oscillations is most expressed on tetrode 1 (T1). The trace epochs within the dashed rectangles represent the maximal amplitude values of the measured oscillation. *C*: comparison of the maximal absolute amplitudes between T1 (*top*) and T2 (*bottom*) LFP_s oscillations during theta (*left*) and spindles (*right*) periods. *D, top*: the averaged relative values of the maximal theta amplitude for all rats are significantly higher for the tetrodes with isolated theta-units (red bar) compared with the tetrodes where no theta-unit was identified (white bar; $P < 0.05$). *Bottom*: averaged relative values of the maximal spindles amplitude for theta-unit (blue bar) and nontheta unit tetrodes (white bar) for the same rats ($P > 0.05$). *E*: comparison of theta (*top*) and spindles (*bottom*) power spectrograms. While both express a spectral power peak around 8Hz (white vertical dashed line), spindles are also characterized by a robust harmonic secondary oscillations at higher frequencies. *F*: the same comparison 24 h later. The black vertical dashed lines denote the same 2 s epochs presented in *A* and *B,* respectively.

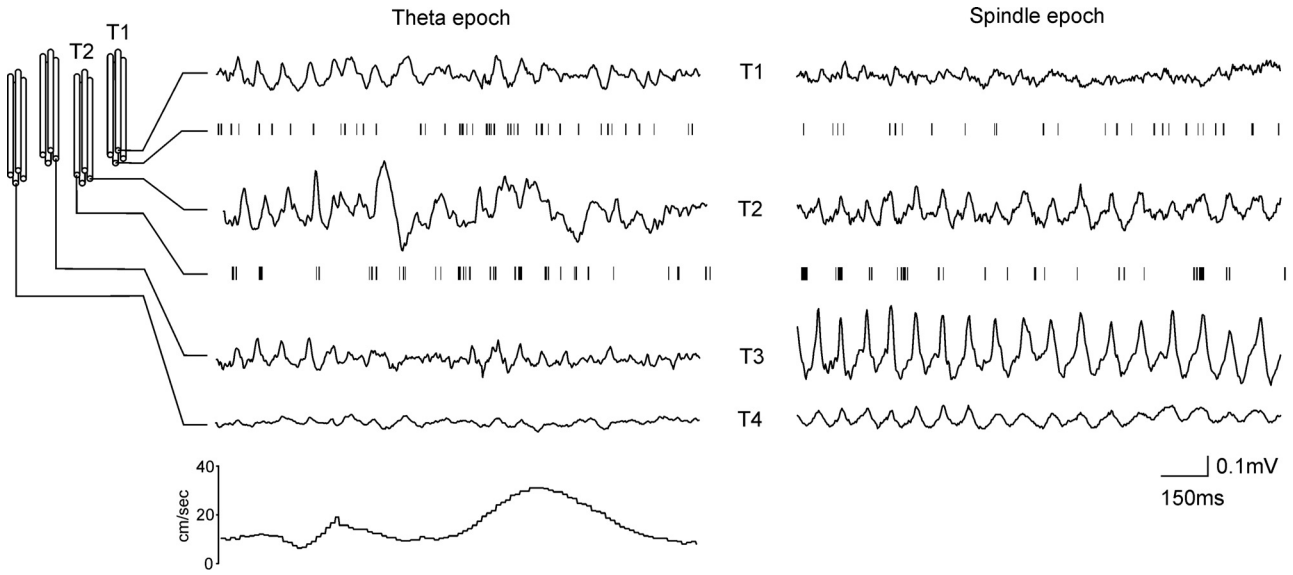

FIG. 5. Theta oscillatory pattern follows the distribution of theta units. Configuration of the implanted tetrodes within AV and an example of concurrent LFP_s signals during theta period (*left*) with 2 theta-unit tetrodes. Theta amplitude is prominent on tetrode 1 (T1) and tetrode 2 (T2), where theta units were isolated, and theta amplitude is well-expressed also on tetrode 3 (T3). *Bottom trace*: the speed of the animal (cm/s). *Right*: the LFP_s signal from the same tetrodes during an inactive behavioral period of the animal. The presence of high-voltage spindles defines this LFP_s epoch as a spindle period. Note the largest spindles amplitude is on T3.

highlight the thalamic origin of the measured theta oscillation, which we conclude is not merely a volume conduction from overlying cortical structures.

We then compared spectral powers for each tetrode between theta and spindle periods. The thalamic reticular nucleus is regarded as a pacemaker of the spindle activity (Steriade et al. 1985), and focal zones within anterior thalamus receive differentiated reticular innervation in rodents (Gonzalo-Ruiz and Lieberman 1995). Electrophysiologically, we found diverse AV spindle amplitudes (from 3 to 280 μV), depending on the electrode tip configuration (Fig. 4, *A* and *B, right*). Spindle oscillations had maximal amplitude values that did not match the maximal theta amplitude values for each tetrode (Fig. 4*C*). Although both oscillations were in the range of 6–11 Hz, the spectral profile of spindles differed from theta. Unlike theta oscillations (Fig. 4, *E* and *F, top*), recorded spindles were robust harmonic oscillations characterized by multiple spectral peaks (Fig. 4, *E* and *F, bottom*). Furthermore, spindle spectral power undergoes a gradual frequency decrease with highest values at the start of the spindle epoch (Fig. 4, *E* and *F*).

We next determined if the amplitude of the spindles is dependent on the amplitude of the preceding theta episodes. To detect corresponding pattern between theta and spindles amplitude, we measured their values for all tetrode channels. We compared maximal amplitude values for all theta epochs to maximal amplitude for all subsequent spindle epochs across all tetrodes (Fig. 6, *A–I*). The relation between the average theta periods values (Fig. 6, *A*, *D,* and *G*) and spindle periods values (*B, E,* and *H*) was measured using the theta-spindles ratio. The theta-spindles ratio for all recordings showed no selectivity of theta unit tetrodes for spindle oscillation amplitudes (Fig. 6, *C, F,* and *I*). The LFP_s mapping of theta spectral power did not correspond with spindle spectral power (Fig. 6, *J* and *K*). The average amplitude of spindle amplitude from a tetrode, detecting a theta unit, has similar values compared with average spindle amplitude from the remaining (nontheta unit) tetrodes (Student's *t*-test $P > 0.05$). Taken together, these data suggest that theta and spindle oscillations within AV are triggered by different inputs.

Ratio of theta to delta spectral powers shares concurrent dynamics in LFP_s and LFP_l recordings

To prove that theta rhythm is not restricted to individual cells but represents the synchronized activity of AV, we needed an LFP signal from a larger thalamic population. A current hypothesis is that the magnitude of LFP oscillations indicates the presence of synchronous synaptic activity and is a measure that averages activity across a region of tissue (Mitzdorf 1985; Murthy and Fetz 1996; Pesaran 2009). We calculated that small-diameter (25 μm) high-impedance electrodes (1–1.5 MΩ) could detect a low-frequency signal from thalamic neurons within ~0.047 mm^3 of thalamic tissue (see METHODS), considering that the extracellular signal decreases as a function of distance from the neuron (Fig. 7). The decay explains why a single neuron had so robust effect on our LFP_s (Fig. 4, *A* and *B*). A similar exponential rule is used to identify extracellular spike signals (Henze et al. 2000). A cylinder with a radius of 47 μm contains on average 1,083 neurons in rat thalamus (Mooney and Miller 2007; Ramos et al. 1995), which is the maximum number of possible recordable cells by a single small-diameter electrode. In this case, the total number of AV theta cells (23.7%) contributing to the LFP_s will be ~257. To evaluate the field oscillatory properties of the anterior thalamus over a larger volume (but still localized to AV), we used a larger-diameter (100 μm), low impedance (50–250 kΩ) electrode. Electrode impedance has very little effect on recording area of LFP, and its effect is restricted mainly to the noise levels (see METHODS). Thus the parameter that allowed us a larger volume recording is the increase in the electrode diameter. Our calculations predict that, in this case, the signal will include the activity of ~1,849 neurons within 0.080 mm^3 of thalamic tissue (see METHODS). As a result, ~440 theta cells will be entrained in the LFP_l signal.

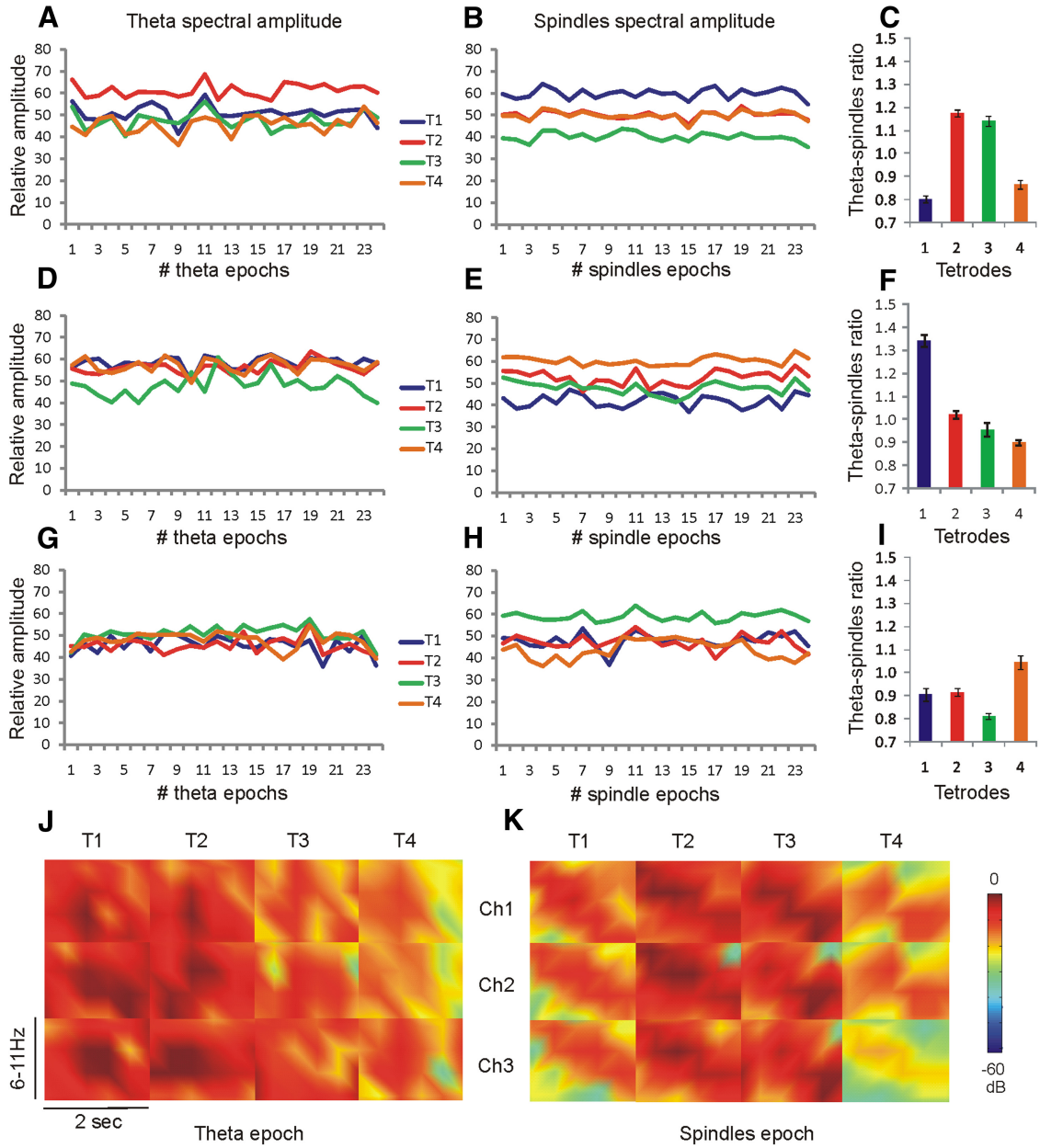

FIG. 6. Local theta amplitude follows an independent distribution from local spindles amplitude. *A*: example of maximal theta spectral power amplitude for all theta epochs for each tetrode per recording session. The different tetrodes are represented with blue (T1), red (T2), green (T3), and orange (T4) colors. The T2 (red line) is also a tetrode with an identified theta unit. Each theta epoch represents concurrently-measured relative theta amplitude (6–11 Hz). *B*: relative maximal spindle amplitude from the same tetrodes over of 25 spindle epochs. *C*: theta-spindles ratio is the ratio between the averaged maximal theta values and averaged maximal spindles values per tetrode. The theta-spindles ratio of theta-unit tetrode (T2) in this case has a similar value to nontheta unit tetrode (T3; $P > 0.05$). *D*: example of maximal theta spectral power amplitude for all theta epochs per recording session with 2 theta-units isolated with T1 and T2. *E*: relative maximal spindles amplitude from the same tetrodes. *F*: the theta-spindles ratio in this case represents a significant difference between both theta-unit tetrodes ($P < 0.01$). *G*: example of the maximal theta spectral power amplitude from all theta epochs per recording session with theta-modulated unit (T2). *H*: the relative maximal spindles amplitude from the same tetrodes. *I*: theta-spindles ratio can be lower or higher for the theta-modulated unit, when comparted to the rest tetrodes. *J*: example of LFP_s power spectrogram map from a fast-spiking theta unit identified on the 1st tetrode (T1). Each rectangle represents color-coded spectral power for the frequency range of 6–11 Hz and duration of 2 s during a theta epoch. Columns denote tetrode number and rows denote the channel number for each tetrode. *K*: LFP_s power spectrogram map for the same rat during a subsequent spindle epoch. Note the tendency of peak frequency to decrease for all channels. The low-expressed spindles amplitude is not specific to T1 channels but is also evident for T4 channels.

Because the AV is composed of nonlayered cells and the net potential difference after simultaneous dendritic activation could be very small, the interpretation of LFP_l is difficult on its own. We therefore compared the signals from small- and large-diameter electrodes implanted in AV during simultaneous recordings. The increase in LFP_l theta oscillation amplitude coincided with the appearance of theta rhythm on the LFP_s from the tetrode that was simultaneously recording a theta unit (Fig. 8*A*). Although the theta epochs revealed temporally concurrent oscillations between LFP_l and LFP_s (Fig. 8*B*), the residual nontheta epochs did not show oscillatory coupling; the correlation of the nontheta signal between LFP_l

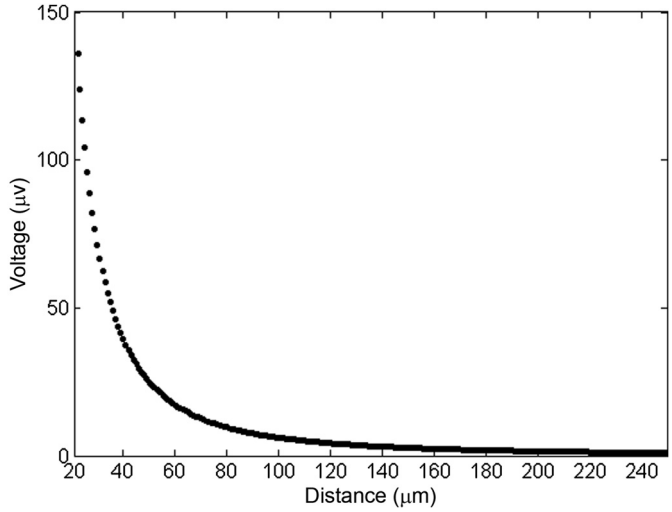

FIG. 7. Exponential distribution of the point source signal. The peak amplitude of the extracellularly detected thalamic unit oscillation (150 μV) decreases exponentially with distance from the center of the electrode.

and LFP_s was not statistically significant (Pearson, $P > 0.05$, $r = 0.0531$, $n = 4$). The correlation of LFP_l and LFP_s signals included epochs with bin size of 1 s for a recording session of 16 min. As the common feature of LFP_l and LFP_s was the detection of theta epochs and considering the fact that the decrease of theta (6–11 Hz) is usually paralleled by an increase of delta (2–4 Hz) (Buzsáki 1996), we decided to evaluate the coherence of LFP_l and LFP_s signals using these two frequencies. The comparative dynamics of theta and delta can be represented as the theta ratio (T-ratio—the ratio of the relative values of theta and delta spectral powers per time bin) (Harris et al. 2002). The values of LFP_l and LFP_s correlated for the entire duration of all recording sessions (Pearson, $P < 0.01$, $r = 0.234$, $n = 4$, Fig. 8, *C–E*). Take together our data propose that thalamic theta rhythm is generated by local oscillations evoked selectively by theta units in anterior thalamus.

DISCUSSION

We have shown that distinct populations of single units can be discriminated in extracellular recordings from AV thalamic nucleus in freely behaving rats. Bursting thalamic units that are highly entrained to limbic theta rhythm (6–11 Hz) comprise 23.7% of AV neurons. These units also determine the amplitude of the local oscillations during theta periods but are uncorrelated with the amplitude of the subsequent spindles. We also found that theta rhythm is a characteristic feature of the LFP_l for AV, which functionally positions anterior thalamus as a part of limbic circuitry.

Classification of AV neurons

We used three independent criteria to differentiate AV neurons in freely behaving rats. These were: ability to burst, average firing frequency, and rhythmic spiking in the theta range (6–11 Hz). We identified a small population of AV neurons (12.5%) that only fire single spikes (which we classified as nonbursting), characterized by a low average firing rate (9.8 ± 5.9 Hz). Depending on the susceptibility to burst, the remaining units were divided into low- and high-probability bursting groups. The low-probability bursting neurons (23.7%) possess a preferentially tonic firing mode, indicated by a high autocorrelation index (27.5 ± 1.8). The high-probability bursting units were subdivided into theta-bursting (35.0%) and nontheta bursting neurons (20.0%).

Rodent AV cells have electrophysiological properties comparable to other thalamic neurons (Pare et al. 1987, 1991). Electron microscope studies of anterior thalamic nuclei reveal two main types of neurons: thalamocortical, which are glutamatergic, and therefore excitatory, and local-circuit GABAergic neurons, the axonal domain of which is located within the limits of the thalamic nuclei (Pare et al. 1991; Somogyi et al. 1978). About half the neurons recorded in our study, namely the low- and high-probability bursting non-theta cells, are likely to be principal (or relay) thalamocortical cells. The narrow shape of the spike of the fast-spiking theta cells (175.1 ± 49.9 μs) as well as their high firing frequency (40.9 ± 15.3 Hz), are suggestive of Golgi type II interneurons (Somogyi et al. 1978). Depending on the average firing rate, we identified slow-spiking (14.9 ± 6.9 Hz) and fast-spiking (40.9 ± 15.3 Hz) theta cells, which comprise 23.7% of the AV units. By comparison, only 7.5% of the units in antero- and laterodorsal thalamic nuclei were classified as theta cells. We also characterized a third, theta-related group in AV with a very low theta index (0.03 ± 0.02) as these theta-modulated cells discharged within theta frequency for only brief periods. In total, we estimated that one third of AV neurons (35.0%) fire in theta-rhythmic mode. This is approximately half the number of theta-related units estimated in rat AV under anesthesia (75%) (Vertes et al. 2001). The electrophysiological characteristics of many neurons vary with the preparation (Steriade 2001b), and the bursting firing patterns of cortical and thalamic cells in nonanesthetized, awake animals (Steriade et al. 2001) can differ substantially from those in anesthetized animals (Nunez et al. 1993; Steriade et al. 1998). Here we confirm AV as a locus of theta-bursting neurons, because one-third of AV units express a theta profile during recordings in freely behaving rats.

Cellular entrainment by local field oscillations

Theta rhythm, which shows power augmentation during behavioral arousal and locomotion, is believed to serve a critical role in the mnemonic functions of the limbic system (Burgess et al. 2002; Hasselmo et al. 2002; Kahana et al. 2001; Kirk and Mackay 2003; Vertes and Kocsis 1997). Inactivation of medial septum abolishes the theta rhythmical discharge in both the hippocampal formation and mammillary bodies (Kirk et al. 1996), which appear to be also the two major regions that provide monosynaptic inputs to anterior thalamus (Ishizuka 2001; Wright et al. 2010). Lesions of hippocampal projections to thalamus have been shown to disrupt the spiking activity of rabbit AV neurons (Smith et al. 2004). This line of research suggests that anterior thalamus is involved in information processing within the medial (theta-related) hippocampo-diencephalic system (Aggleton et al. 2010; Vann and Aggleton 2004). Our data, which reveal the theta properties of anteroventral nucleus, support this view.

Neuronal bursts in thalamic nuclei can occur during waking states, although bursting is more prevalent than during slow-wave sleep (Fanselow et al. 2001; Guido and Weyand 1995;

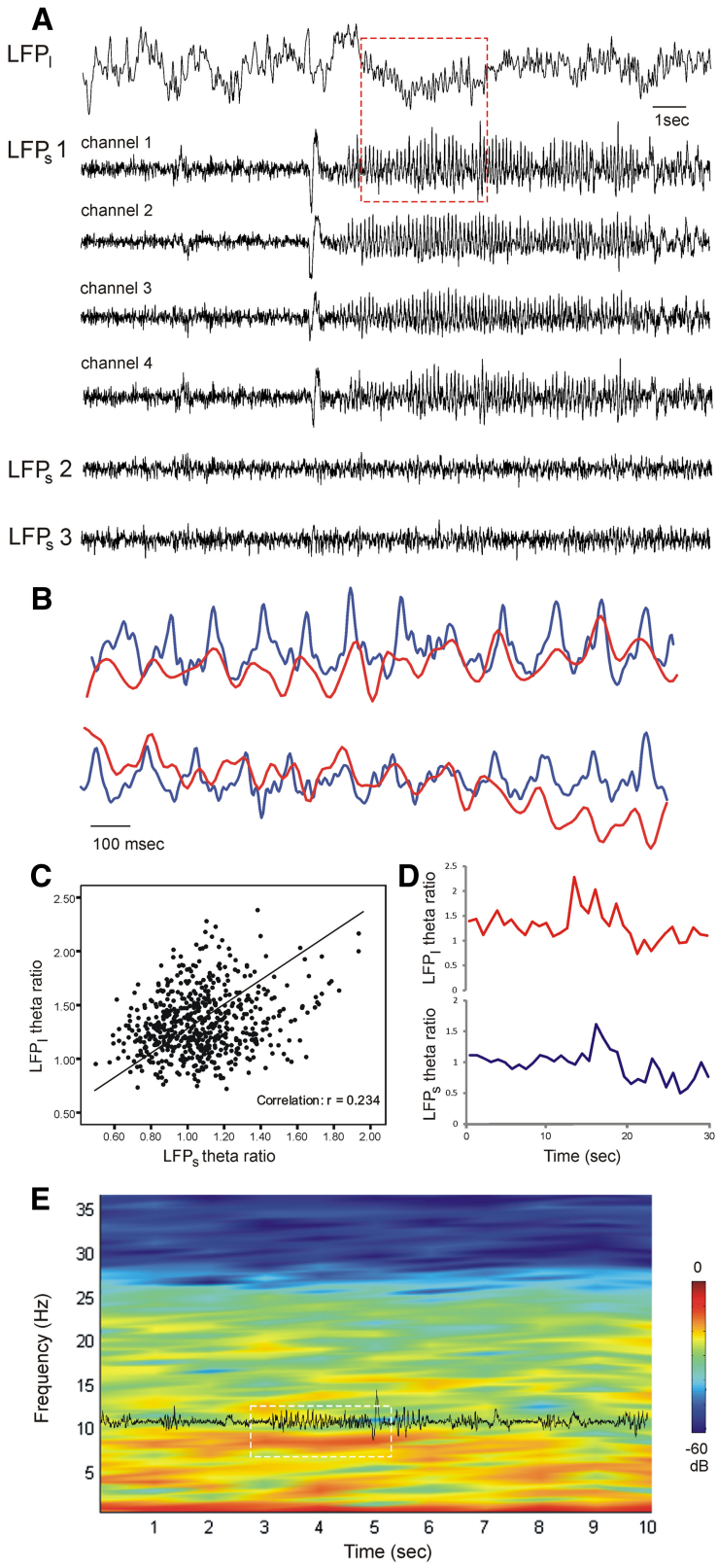

FIG. 8. Large- and small-diameter signals undergo parallel alternations of theta amplitude. *A*: example of parallel AV recording with low- and high-impedance electrodes during theta periods. *Top*: large-diameter local field potential (LFP$_l$). *Bottom*: LFP$_s$ detected from different tetrodes. The signal from tetrode one (LFP$_s$1) is represented by all four channels. The same tetrode simultaneously isolates a fast-spiking theta unit. Note the lack of theta oscillations in the signals from the 2nd and 3rd tetrodes (LFP$_s$2 and LFP$_s$3, respectively). The red rectangle marks the concurrent occurrence of the theta epoch in LFP$_l$ and LFP$_s$1. *B*: magnified image of the LFP$_l$ (red trace) and LFP$_s$1, channel 1 (blue trace) from the marked theta epoch in *A*. Top and lower pairs are subsequent epochs. *C*: a positive correlation is evident between LFP$_l$ and LFP$_s$1 for the theta ratio (theta- over delta spectral amplitude) evaluated in epochs with a bin size of 1 s. *D*: example of coherent alternations of LFP$_l$ (top red trace) and LFP$_s$1 (bottom blue trace) theta ratios. The brief increase denotes the occurrence of theta epoch. *E*: low-impedance power spectrogram with a temporally superimposed LFP$_s$ trace. The white rectangle marks a theta period with a simultaneous increase of spectral power in the 6–11 Hz range and augmentation of oscillatory amplitude.

Reinagel et al. 1999; Swadlow and Gusev 2001; Weyand et al. 2001). Thalamic theta units in our experiments fired in bursts more often during waking states (particularly locomotion-related periods), suggesting these units are component of the limbic circuit. However, to define AV theta units as typical limbic theta cells, we needed to obtain information about their relation to the oscillatory field properties of anterior thalamus, particularly theta rhythm. Although recent research has demonstrated the possibility of exploiting the relationship between LFPs and individual spiking (Katzner et al. 2009; Logothetis et

al. 2007), LFP interpretation faces the difficulty of estimating the volume of involved neuronal tissue. To demonstrate that the theta signal is of local origin and not a contaminated signal from distant structures, we used small-diameter (25 μm) high-impedance tetrodes (1–1.5 MΩ). Importantly, the observed LFP_s oscillatory amplitude strongly differed when compared for all tetrodes. We found that theta units reflected the amplitude of the LFP during theta periods, which were characterized by high locomotor activity. The theta-unit tetrodes corresponded to higher values of theta amplitude compared with the tetrodes, which could not discriminate theta units.

To demonstrate the selective effect of theta cells on limbic theta but not on other thalamic oscillations, we examined their relation to spindles. Spindle oscillations, which predominantly occur during the early stages of sleep, are generated by thalamic circuits (Steriade et al. 1985). In contrast to delta and slow oscillations, which are also feature of other brain regions such as hippocampal formation, spindles are generated exclusively by thalamocortical interactions (Contreras and Steriade 1996, 1997; Contreras et al. 1996, 1997a). We reveal that LFP theta zones are formed differently when compared with the spindle amplitude distribution during subsequent behaviorally inactive periods. While theta unit tetrodes obtained the highest theta spectral power, the same tetrodes were not necessarily linked to the lowest spindle spectral power. As the theta unit tetrodes lacked the selective increase of theta-spindles ratio (maximal theta over maximal spindles) compared with the remaining tetrodes, we concluded that thalamic fast-and slow-spiking theta cells selectively determine the spectral amplitude of limbic theta oscillation. The thalamic reticular nucleus plays a key role as the generator and pacemaker of the thalamic spindle waves (Steriade et al. 1985, 1987), and the rat anterior thalamic nuclei receive a heavy input from cell groups in the ipsilateral rostral reticular nucleus (Gonzalo-Ruiz and Lieberman 1995). The occurrence of thalamic spindles in AV is demonstrated by the comparative finding that the cat anterior thalamic group, which is devoid of reticular input, does not display spindling oscillations (Pare et al. 1987). Our finding that theta and spindle oscillations differ in their spatial distribution within AV suggests that the reticular nucleus does not control theta rhythm in anterior thalamus. We also observed that AV spindles are harmonic oscillations with a dominant frequency in the range of 7–10 Hz, and the value of this frequency gradually decreases after the onset of the spindling epoch (Mackenzie et al. 2005; Sitnikova et al. 2009). Thalamic spindle periods occur during global inhibition of thalamocortical neurons by the thalamic reticular nucleus (Diekelmann and Born 2010; Steriade 2001a). This allowed us to explore thalamic theta cells during their inhibited mode, where the AV theta units exhibited less bursting and higher degree of tonic spiking during the spindle periods. We did not observe periods with theta oscillations during sleep recordings. This finding supports the oscillatory profile of thalamic sleep rhythms, characterized by spindles during slow-wave sleep and lack of theta rhythm during the REM phase (Pace-Schott and Hobson 2002; Steriade 1997; Steriade et al. 1993).

In summary, the present data together with previous studies (Albo et al. 2003; Smith et al. 2004), suggest that the theta signal integrates functionally the anterior thalamus in the hippocampo-diencephalic circuitry, damage to which can cause diencephalic amnesia (Aggleton and Sahgal 1993; Gold and Squire 2006; Harding et al. 2000).

ACKNOWLEDGMENTS

We thank V. Hok for comments on earlier versions of the manuscript.

GRANTS

This work was supported by a Wellcome Trust Grant 081075 to J. P. Aggleton, S. M. O'Mara, J. T. Erichsen, and S. D. Vann.

DISCLOSURES

No conflicts of interest, financial or otherwise, are declared by the author(s).

REFERENCES

Aggleton JP, O'Mara SM, Vann SD, Wright NF, Tsanov M, Erichsen JT. Hippocampal-anterior thalamic pathways for memory: uncovering a network of direct and indirect actions. *Eur J Neurosci* 31: 2292–2307, 2010.

Aggleton JP, Sahgal A. The contribution of the anterior thalamic nuclei to anterograde amnesia. *Neuropsychologia* 31: 1001–1019, 1993.

Albo Z, Viana Di Prisco G, Vertes RP. Anterior thalamic unit discharge profiles and coherence with hippocampal theta rhythm *Thalamus Related Syst* 2: 133–144, 2003.

Anderson MI, O'Mara SM. Analysis of recordings of single-unit firing and population activity in the dorsal subiculum of unrestrained, freely moving rats. *J Neurophysiol* 90: 655–665, 2003.

Berke JD, Okatan M, Skurski J, Eichenbaum HB. Oscillatory entrainment of striatal neurons in freely moving rats. *Neuron* 43: 883–896, 2004.

Bland BH, Konopacki J, Kirk IJ, Oddie SD, Dickson CT. Discharge patterns of hippocampal theta-related cells in the caudal diencephalon of the urethan-anesthetized rat. *J Neurophysiol* 74: 322–333, 1995.

Burgess N, Maguire EA, O'Keefe J. The human hippocampus and spatial and episodic memory. *Neuron* 35: 625–641, 2002.

Buzsáki G. The hippocampo-neocortical dialogue. *Cereb Cortex* 6: 81–92, 1996.

Buzsáki G. Theta oscillations in the hippocampus. *Neuron* 33: 325–340, 2002.

Buzsaki G. Large-scale recording of neuronal ensembles. *Nat Neurosci* 7: 446–451, 2004.

Buzsáki G. Theta rhythm of navigation: link between path integration and landmark navigation, episodic and semantic memory. *Hippocampus* 15: 827–840, 2005.

Contreras D, Destexhe A, Sejnowski TJ, Steriade M. Control of spatiotemporal coherence of a thalamic oscillation by corticothalamic feedback. *Science* 274: 771–774, 1996.

Contreras D, Destexhe A, Sejnowski TJ, Steriade M. Spatiotemporal patterns of spindle oscillations in cortex and thalamus. *J Neurosci* 17: 1179–1196, 1997a.

Contreras D, Destexhe A, Steriade M. Intracellular and computational characterization of the intracortical inhibitory control of synchronized thalamic inputs in vivo. *J Neurophysiol* 78: 335–350, 1997b.

Contreras D, Steriade M. Spindle oscillation in cats: the role of corticothalamic feedback in a thalamically generated rhythm. *J Physiol* 490: 159–179, 1996.

Contreras D, Steriade M. Synchronization of low-frequency rhythms in corticothalamic networks. *Neuroscience* 76: 11–24, 1997.

Csicsvari J, Henze DA, Jamieson B, Harris KD, Sirota A, Bartho P, Wise KD, Buzsaki G. Massively parallel recording of unit and local field potentials with silicon-based electrodes. *J Neurophysiol* 90: 1314–1323, 2003.

Csicsvari J, Hirase H, Czurko A, Buzsáki G. Reliability and state dependence of pyramidal cell-interneuron synapses in the hippocampus: an ensemble approach in the behaving rat. *Neuron* 21: 179–189, 1998.

Csicsvari J, Hirase H, Czurko A, Mamiya A, Buzsaki G. Oscillatory coupling of hippocampal pyramidal cells and interneurons in the behaving rat. *J Neurosci* 19: 274–287, 1999.

Deschenes M, Paradis M, Roy JP, Steriade M. Electrophysiology of neurons of lateral thalamic nuclei in cat: resting properties and burst discharges. *J Neurophysiol* 51: 1196–1219, 1984.

Diekelmann S, Born J. The memory function of sleep. *Nat Rev Neurosci* 11: 114–126, 2010.

Fanselow EE, Sameshima K, Baccala LA, Nicolelis MA. Thalamic bursting in rats during different awake behavioral states. *Proc Natl Acad Sci USA* 98: 15330–15335, 2001.

Fuentealba P, Timofeev I, Steriade M. Prolonged hyperpolarizing potentials precede spindle oscillations in the thalamic reticular nucleus. *Proc Natl Acad Sci USA* 101: 9816–9821, 2004.

Gold JJ, Squire LR. The anatomy of amnesia: neurohistological analysis of three new cases. *Learn Mem* 13: 699–710, 2006.

Gonzalo-Ruiz A, Lieberman AR. Topographic organization of projections from the thalamic reticular nucleus to the anterior thalamic nuclei in the rat. *Brain Res Bull* 37: 17–35, 1995.

Gray CM, Maldonado PE, Wilson M, McNaughton B. Tetrodes markedly improve the reliability and yield of multiple single-unit isolation from multi-unit recordings in cat striate cortex. *J Neurosci Methods* 63: 43–54, 1995.

Guido W, Weyand T. Burst responses in thalamic relay cells of the awake behaving cat. *J Neurophysiol* 74: 1782–1786, 1995.

Harding A, Halliday G, Caine D, Kril J. Degeneration of anterior thalamic nuclei differentiates alcoholics with amnesia. *Brain* 123: 141–154, 2000.

Harris KD, Csicsvari J, Hirase H, Dragoi G, Buzsaki G. Organization of cell assemblies in the hippocampus. *Nature* 424: 552–556, 2003.

Harris KD, Henze DA, Hirase H, Leinekugel X, Dragoi G, Czurko A, Buzsáki G. Spike train dynamics predicts theta related phase precession in hippocampal pyramidal cells. *Nature* 417: 738–741, 2002.

Hasselmo ME, Bodelon C, Wyble BP. A proposed function for hippocampal theta rhythm: separate phases of encoding and retrieval enhance reversal of prior learning. *Neural Comput* 14: 793–817, 2002.

Hasselmo ME, Eichenbaum H. Hippocampal mechanisms for the context-dependent retrieval of episodes. *Neural Netw* 18: 1172–1190, 2005.

Henze DA, Borhegyi Z, Csicsvari J, Mamiya A, Harris KD, Buzsaki G. Intracellular features predicted by extracellular recordings in the hippocampus in vivo. *J Neurophysiol* 84: 390–400, 2000.

Huigen E, Peper A, Grimbergen CA. Investigation into the origin of the noise of surface electrodes. *Med Biol Eng Comput* 40: 332–338, 2002.

Ishizuka N. Laminar organization of the pyramidal cell layer of the subiculum in the rat. *J Comp Neurol* 435: 89–110, 2001.

Jahnsen H, Llinas R. Electrophysiological properties of guinea-pig thalamic neurones: an in vitro study. *J Physiol* 349: 205–226, 1984a.

Jahnsen H, Llinas R. Ionic basis for the electro-responsiveness and oscillatory properties of guinea-pig thalamic neurons in vitro. *J Physiol* 349: 227–247, 1984b.

Jones EG editor. *The Thalamus.* New York: Plenum, 1985.

Kahana MJ, Seelig D, Madsen JR. Theta returns. *Curr Opin Neurobiol* 11: 739–744, 2001.

Katzner S, Nauhaus I, Benucci A, Bonin V, Ringach DL, Carandini M. Local origin of field potentials in visual cortex. *Neuron* 61: 35–41, 2009.

Kirk IJ, Mackay JC. The role of theta-range oscillations in synchronising and integrating activity in distributed mnemonic networks. *Cortex* 39: 993–1008, 2003.

Kirk IJ, Oddie SD, Konopacki J, Bland BH. Evidence for differential control of posterior hypothalamic, supramammillary, and medial mammillary theta-related cellular discharge by ascending and descending pathways. *J Neurosci* 16: 5547–5554, 1996.

Klausberger T, Magill PJ, Marton LF, Roberts JD, Cobden PM, Buzsaki G, Somogyi P. Brain-state- and cell-type-specific firing of hippocampal interneurons in vivo. *Nature* 421: 844–848, 2003.

Kreiman G, Hung CP, Kraskov A, Quiroga RQ, Poggio T, DiCarlo JJ. Object selectivity of local field potentials and spikes in the macaque inferior temporal cortex. *Neuron* 49: 433–445, 2006.

Logothetis NK, Kayser C, Oeltermann A. In vivo measurement of cortical impedance spectrum in monkeys: implications for signal propagation. *Neuron* 55: 809–823, 2007.

Mackenzie L, Pope KJ, Willoughby JO. Gamma rhythms are not integral to EEG spindle phenomena. *Clin Neurophysiol* 116: 861–870, 2005.

Mitzdorf U. Current source-density method and application in cat cerebral cortex: investigation of evoked potentials and EEG phenomena. *Physiol Rev* 65: 37–100, 1985.

Mooney SM, Miller MW. Postnatal generation of neurons in the ventrobasal nucleus of the rat thalamus. *J Neurosci* 27: 5023–5032, 2007.

Murthy VN, Fetz EE. Synchronization of neurons during local field potential oscillations in sensorimotor cortex of awake monkeys. *J Neurophysiol* 76: 3968–3982, 1996.

Nelson MJ, Pouget P, Nilsen EA, Patten CD, Schall JD. Review of signal distortion through metal microelectrode recording circuits and filters. *J Neurosci Methods* 169: 141–157, 2008.

Nunez A, Amzica F, Steriade M. Electrophysiology of cat association cortical cells in vivo: intrinsic properties and synaptic responses. *J Neurophysiol* 70: 418–430, 1993.

Pace-Schott EF, Hobson JA. The neurobiology of sleep: genetics, cellular physiology and subcortical networks. *Nat Rev Neurosci* 3: 591–605, 2002.

Pare D, Dossi RC, Steriade M. Three types of inhibitory postsynaptic potentials generated by interneurons in the anterior thalamic complex of cat. *J Neurophysiol* 66: 1190–1204, 1991.

Pare D, Steriade M, Deschenes M, Oakson G. Physiological characteristics of anterior thalamic nuclei, a group devoid of inputs from reticular thalamic nucleus. *J Neurophysiol* 57: 1669–1685, 1987.

Parker A, Gaffan D. The effect of anterior thalamic and cingulate cortex lesions on object-in-place memory in monkeys. *Neuropsychologia* 35: 1093–1102, 1997.

Pesaran B. Uncovering the mysterious origins of local field potentials. *Neuron* 61: 1–2, 2009.

Pettersen KH, Einevoll GT. Amplitude variability and extracellular low-pass filtering of neuronal spikes. *Biophys J* 94: 784–802, 2008.

Ramos R, Requena V, Diaz F, Villena A, Perez de Vargas I. Evolution of neuronal density in the ageing thalamic reticular nucleus. *Mech Ageing Dev* 83: 21–29, 1995.

Reinagel P, Godwin D, Sherman SM, Koch C. Encoding of visual information by LGN bursts. *J Neurophysiol* 81: 2558–2569, 1999.

Royer S, Sirota A, Patel J, Buzsaki G. Distinct representations and theta dynamics in dorsal and ventral hippocampus. *J Neurosci* 30: 1777–1787, 2010.

Sitnikova E, Hramov AE, Koronovsky AA, van Luijtelaar G. Sleep spindles and spike-wave discharges in EEG: Their generic features, similarities and distinctions disclosed with Fourier transform and continuous wavelet analysis. *J Neurosci Methods* 180: 304–316, 2009.

Smith DM, Wakeman D, Patel J, Gabriel M. Fornix lesions impair context-related cingulothalamic neuronal patterns and concurrent discrimination learning in rabbits (*Oryctolagus cuniculus*). *Behav Neurosci* 118: 1225–1239, 2004.

Somogyi G, Hajdu F, Tombol T. Ultrastructure of the anterior ventral and anterior medial nuclei of the cat thalamus. *Exp Brain Res* 31: 417–431, 1978.

Steriade M. Synchronized activities of coupled oscillators in the cerebral cortex and thalamus at different levels of vigilance. *Cereb Cortex* 7: 583–604, 1997.

Steriade M. Active neocortical processes during quiescent sleep. *Arch Ital Biol* 139: 37–51, 2001a.

Steriade M. Impact of network activities on neuronal properties in corticothalamic systems. *J Neurophysiol* 86: 1–39, 2001b.

Steriade M, Deschenes M, Domich L, Mulle C. Abolition of spindle oscillations in thalamic neurons disconnected from nucleus reticularis thalami. *J Neurophysiol* 54: 1473–1497, 1985.

Steriade M, Domich L, Oakson G, Deschenes M. The deafferented reticular thalamic nucleus generates spindle rhythmicity. *J Neurophysiol* 57: 260–273, 1987.

Steriade M, Jones EG, McCormik DA editors. *Thalamus. Organisation and Function.* Oxford, UK: Elsevier, 1997.

Steriade M, McCormick DA, Sejnowski TJ. Thalamocortical oscillations in the sleeping and aroused brain. *Science* 262: 679–685, 1993.

Steriade M, Timofeev I, Durmuller N, Grenier F. Dynamic properties of corticothalamic neurons and local cortical interneurons generating fast rhythmic (30–40 Hz) spike bursts. *J Neurophysiol* 79: 483–490, 1998.

Steriade M, Timofeev I, Grenier F. Natural waking and sleep states: a view from inside neocortical neurons. *J Neurophysiol* 85: 1969–1985, 2001.

Swadlow HA, Gusev AG. The impact of "bursting" thalamic impulses at a neocortical synapse. *Nat Neurosci* 4: 402–408, 2001.

Taube JS. Head direction cells recorded in the anterior thalamic nuclei of freely moving rats. *J Neurosci* 15: 70–86, 1995.

Taube JS. The head direction signal: origins and sensory-motor integration. *Annu Rev Neurosci* 30: 181–207, 2007.

Vann SD, Aggleton JP. The mammillary bodies: two memory systems in one? *Nat Rev Neurosci* 5: 35–44, 2004.

Vertes RP, Albo Z, Viana Di Prisco G. Theta-rhythmically firing neurons in the anterior thalamus: implications for mnemonic functions of Papez's circuit. *Neuroscience* 104: 619–625, 2001.

Vertes RP, Kocsis B. Brainstem-diencephalo-septohippocampal systems controlling the theta rhythm of the hippocampus. *Neuroscience* 81: 893–926, 1997.

Warburton EC, Baird A, Morgan A, Muir JL, Aggleton JP. The conjoint importance of the hippocampus and anterior thalamic nuclei for allocentric spatial learning: evidence from a disconnection study in the rat. *J Neurosci* 21: 7323–7330, 2001.

Weyand TG, Boudreaux M, Guido W. Burst and tonic response modes in thalamic neurons during sleep and wakefulness. *J Neurophysiol* 85: 1107–1118, 2001.

Wilson MA, McNaughton BL. Dynamics of the hippocampal ensemble code for space. *Science* 261: 1055–1058, 1993.

Wright NF, Erichsen JT, Vann SD, O'Mara SM, Aggleton JP. Parallel but separate inputs from limbic cortices to the mammillary bodies and anterior thalamic nuclei in the rat. *J Comp Neurol* 518: 2334–2354, 2010.

Ylinen A, Bragin A, Nadasdy Z, Jando G, Szabo I, Sik A, Buzsaki G. Sharp wave-associated high-frequency oscillation (200 Hz) in the intact hippocampus: network and intracellular mechanisms. *J Neurosci* 15: 30–46, 1995.